Nondestructive Rydberg parity meter and its applications

S.-L. Su,[1,*] Fu-Qiang Guo,[1] L. Tian,[1] X.-Y. Zhu,[1,2] L.-L. Yan,[1] E.-J. Liang,[1] and M. Feng[1,3,4,†]

[1]*School of Physics, Zhengzhou University, Zhengzhou 450001, China*

[2]*College of Science, Henan University of Engineering, Zhengzhou 451191, China*

[3]*State Key Laboratory of Magnetic Resonance and Atomic and Molecular Physics, Wuhan Institute of Physics and Mathematics, Chinese Academy of Sciences, Wuhan 430071, China*

[4]*Department of Physics, Zhejiang Normal University, Jinhua 321004, China*

(Received 14 October 2019; revised manuscript received 23 December 2019; published 30 January 2020)

Parity meters, utilized to distinguish bipartite quantum states with even or odd parity, have many applications in quantum information processing. We propose a potentially practical scheme to construct the nondestructive Rydberg parity meter (NRPM) in ground-state subspace using Rydberg atoms. Based on the proposed NRPM, the parity of the qubit atoms could be known in a deterministic and nondestructive way, implying that the output state of the NRPM can be further used in the rest of the process for quantum information tasks. In addition, we study the applications of the proposed NRPM in entangled state fusion, entangled state analysis, and quantum teleportation, as well as quantum logic gate in a decoherence-free subspace regarding collective-dephasing errors. We analyze the performance of the NRPM under the influence of decoherence and consider more general situations for the feasibility of the scheme.

DOI: 10.1103/PhysRevA.101.012347

I. INTRODUCTION

Neutral atoms exhibit strong Rydberg-Rydberg interaction (RRI) when excited to Rydberg states [1–5]. The most interesting phenomenon induced by RRI is the Rydberg blockade, i.e., more than one atom to be excited by the frequency-matched resonant laser is blockaded if the line width of the excitation is significantly narrower than the energy shift caused by the RRI [6,7]. Experimentally, the Rydberg blockade has been observed [8,9], and, furthermore, quantum controlled-NOT gates as well as quantum entangled states [10–18] using Rydberg atoms have also been achieved.

Another interesting quantum operation, called the parity meter [19–25], is useful for quantum computation [19,20] and other quantum information tasks, such as distilling and purifying entangled states [22], analyzing entangled states [21], and protecting quantum memories [26]. Recently parity meters were also used experimentally to prepare the entangled states [24] and observe the jumps of photon number [25] in circuit QED. In addition, using Rydberg atoms, operations to measure many-body parity between the ground state and the Rydberg state were carried out to observe the lower bound of the many-body coherence in combination with unitary operations changing the measurement bases [27]. Moreover, the four-body parity constraints with enhanced Rydberg dressing were employed for constructing an experimentally feasible Lechner-Hauke-Zoller architecture Hamiltonian in a quantum annealer [28].

The parity meter works as follows. For a two-qubit system initially in the state

$$|\psi\rangle_{\text{initial}} = (\alpha|00\rangle + \beta|01\rangle + \gamma|10\rangle + \delta|11\rangle)/\mathcal{N}, \quad (1)$$

with $\mathcal{N}$ the normalization parameter, the parity meter applied on Eq. (1) yields the final state as

$$|\psi\rangle_{\text{even}} = (\alpha|00\rangle + \delta|11\rangle)/\mathcal{N}_- \quad (2)$$

for even parity or

$$|\psi\rangle_{\text{odd}} = (\beta|01\rangle + \gamma|10\rangle)/\mathcal{N}_+ \quad (3)$$

for odd parity, where $\mathcal{N}_-$ and $\mathcal{N}_+$ denote the normalization parameters.

In this work, we propose an experimentally feasible scheme to achieve the two-qubit nondestructive Rydberg parity meter (NRPM) using Rydberg atoms. As presented below, the NRPM can be applied to various quantum information tasks, such as the entangled state fusion, entangled state analysis, quantum teleportation, and quantum logic gate in collective dephasing a decoherence-free subspace (DFS). Our study may broaden the applications of the Rydberg atoms in quantum information processing.

II. RYDBERG PARITY METER

As sketched in Fig. 1(a), the NRPM involves two atoms encoded as qubits and another atom as the auxiliary. The Hamiltonian of the qubit atoms in the interaction picture is

$$\hat{H} = \sum_{j=1,2} \frac{\Omega}{2}(|0\rangle_j\langle R| + |1\rangle_j\langle r|)e^{i\Delta t} + V_{\text{dd}}|rR\rangle\langle Rr| + \text{H.c.} + \sum_{m=R,r}\sum_{n=R,r} V_{mn}|mn\rangle\langle mn|, \quad (4)$$

*slsu@zzu.edu.cn
†mangfeng@wipm.ac.cn

 ©2020 American Physical Society

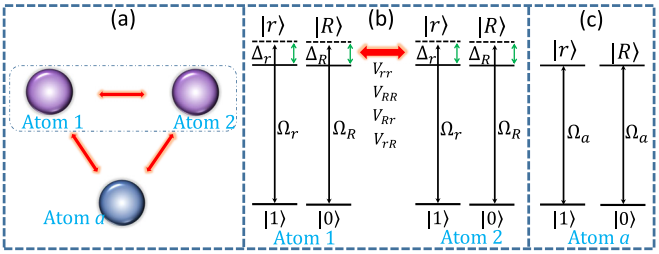

FIG. 1. (a) Schematic of the NRPM, where three Rydberg atoms are located equidistantly as a triangle. Rydberg atoms 1 and 2 are encoded as qubits, while Rydberg atom a works as the auxiliary to acquire the parity information of the qubit atoms 1 and 2. (b) Level structure of two qubit atoms under the laser drives, where the ground state $|0\rangle$ ($|1\rangle$) is coupled to the Rydberg state $|R\rangle$ ($|r\rangle$) with the Rabi frequency Ω_R (Ω_r) and the blue detuning Δ_R (Δ_r). V_{mn} denotes the vdW-type RRI between Rydberg states $|m\rangle$ and $|n\rangle$. (c) Level structure of the auxiliary atom a under the laser drive, with initial state $|+\rangle = (|0\rangle + |1\rangle)/\sqrt{2}$. $|1\rangle$ ($|0\rangle$) coupled to $|r\rangle$ ($|R\rangle$) with Rabi frequency Ω_a. $|0\rangle$ and $|1\rangle$ are ground states. We set $\Delta_R = \Delta_r = \Delta$ and $\Omega_R = \Omega_r = \Omega$ for simplicity, and $\Delta \gg \Omega$ should be satisfied.

in which V_{mn} and $V_{\rm dd}$ denote the van der Waals (vdW) and dipole-dipole interactions, respectively. The dipole-dipole interaction between $|R\rangle$ and $|r\rangle$ with strength V_{dd} could be minimized to zero by choosing both of these two Rydberg states in s state due to the selection rule. Also, the dipole-dipole interaction between any of these two Rydberg states and any other Rydberg states should be much smaller than the vdW interaction, implying the interatomic distance larger than the characteristic length scale R_c [2].

For simplicity, we first set $V_{RR} = V_{rr} = V$ (the situation beyond this simplification will be discussed later in the Discussion) and $V_{rR} = V_{Rr} = V'$. If the condition $\Delta = V/2 \gg \Omega$ is satisfied, the effective couplings between $|00\rangle$ and $|RR\rangle$ and between $|11\rangle$ and $|rr\rangle$ are both achieved with the same coupling strength Ω^2/Δ due to the Rydberg antiblockade [29,30]. But the excitations from $|01\rangle$ to $|Rr\rangle$ and from $|10\rangle$ to $|Rr\rangle$ are inhibited due to the fact of $2\Delta - V' \gg \Omega$. If we drive these two atoms with the time interval $t = \pi\Delta/\Omega^2$, the two atoms initially in the same ground state could be excited to the two-excitation Rydberg state, whereas the two atoms initially in different ground states keep invariant (see Fig. 2).

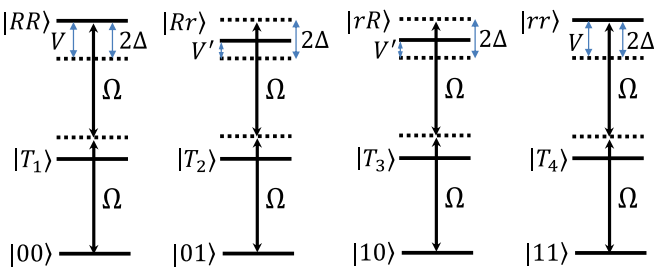

FIG. 2. Excitations in steps (i) and (iii) for the proposed NRPM. The system dynamics of even parity is governed by Rydberg antiblockade mechanism, while that of odd parity is blocked due to the large detuning. The Stark-shift-induced phase could be discarded due to the symmetry of the different components for the parity state. $|T_1\rangle = (|0R\rangle + |R0\rangle)/\sqrt{2}$, $|T_2\rangle = (|0r\rangle + |R1\rangle)/\sqrt{2}$, $|T_3\rangle = (|r0\rangle + |1R\rangle)/\sqrt{2}$, $|T_4\rangle = (|0r\rangle + |r0\rangle)/\sqrt{2}$.

Then we drive the auxiliary atom to the Rydberg state with a π pulse. Due to the Rydberg blockade, the final state of the auxiliary atom depends on the initial parity information of the qubit atom. As such, we can get the information through measuring the state of the auxiliary atom.

Concretely, constructing the nondestructive NRPM consists of the following three steps.

Step (i): Turn on the lasers to drive the qubit atoms 1 and 2 with the time interval $t = \pi\Delta/\Omega^2$. As stated above, the even state would be excited due to the Rydberg antiblockade, whereas the large detuning keeps the odd state to be invariant. In this case, under the conditions of $V_{dd} = 0$, $\Delta = V/2$, $V - V' \gg \Omega$, and $V \gg \Omega$, Eq. (4) reduces to

$$\hat{H}_{\rm eff} = \frac{\Omega^2}{2\Delta}[(|00\rangle\langle RR| + |11\rangle\langle rr| + \text{H.c.})], \tag{5}$$

in a rotating frame with respect to $\hat{U}_{\rm rot} = e^{iV(|rr\rangle\langle rr| + |RR\rangle\langle RR|)t}$. We have ignored the states in single-excitation subspace because they do not exchange energy with the other states and also considered $|00\rangle\langle 00| + |01\rangle\langle 01| + |10\rangle\langle 10| + |11\rangle\langle 11| = \hat{\boldsymbol{I}}$ in computational subspace. By this step, the whole system evolves as

$$\begin{aligned}&(\alpha|00\rangle + \beta|01\rangle + \gamma|10\rangle + \delta|11\rangle)_{12} \otimes (|0\rangle + |1\rangle)_a \\ &\quad\to (\alpha|RR\rangle + \beta|01\rangle + \gamma|10\rangle + \delta|rr\rangle)_{12} \otimes (|0\rangle + |1\rangle)_a.\end{aligned} \tag{6}$$

Step (ii): Turn on the resonant laser to drive the atom a with the time interval $t_a = 2\pi\Omega_a$. Since the qubit atoms initially in an odd-parity state could not be excited after step (i), this drive makes the atom a with the transitions $|0\rangle_a \to -|0\rangle_a$ and $|1\rangle_a \to -|1\rangle_a$. In contrast, if the qubit atoms are initially in the state $|00\rangle$, they would be excited to $|RR\rangle$ after step (i). Then in step (ii), under the conditions of $2V \gg \Omega_a$ and $2V' \ll \Omega_a$, the coupling $|0\rangle_a \to |R\rangle_a$ is blocked while the transition $|1\rangle_a \to -|1\rangle_a$ is achieved. Here we have supposed that the auxiliary atom is identical to the qubit atoms, and thus the RRI is accumulated by a factor 2. Similarly, if the qubit atoms are initially in state $|11\rangle$, they would be excited to $|rr\rangle$ after step (i). In this case the coupling $|1\rangle_a \to |r\rangle_a$ is also blocked while $|0\rangle_a \to -|0\rangle_a$ is achieved in (ii). In addition, the qubit states $|RR\rangle$ and $|rr\rangle$ acquire a phase e^{-iVt_a} due to the RRIs. In short, the evolution of the whole system would be

$$\begin{aligned}&(\alpha|RR\rangle + \beta|01\rangle + \gamma|10\rangle + \delta|rr\rangle)_{12} \otimes (|0\rangle + |1\rangle)_a \\ &\quad\to e^{-iVt_a}(\alpha|RR\rangle - \delta|rr\rangle)_{12} \otimes (|0\rangle - |1\rangle)_a \\ &\qquad - (\beta|01\rangle + \gamma|10\rangle) \otimes (|0\rangle + |1\rangle)_a.\end{aligned} \tag{7}$$

Then we perform the measurement operation on atom a by the basis $|\pm\rangle_a = (|0\rangle_a \pm |1\rangle_a)/\sqrt{2}$. The result $|+\rangle_a$ corresponds to the qubit atoms in $(\beta|01\rangle + \gamma|10\rangle)/\mathcal{N}_+$. Otherwise, the qubit atoms collapse to $(\alpha|RR\rangle - \delta|rr\rangle)/\mathcal{N}_-$ after discarding the global phase.

Step (iii): Perform the inverse operations of step (i) as well as the single-qubit operation $|1\rangle_1 \to -|1\rangle_1$. The evolution of the qubit atoms would be

$$\begin{aligned}&(\beta|01\rangle + \gamma|10\rangle)/\mathcal{N}_+ \to (\beta|01\rangle + \gamma|10\rangle)/\mathcal{N}_+, \\ &(\alpha|RR\rangle - \delta|rr\rangle)/\mathcal{N}_- \to (\alpha|00\rangle + \delta|11\rangle)/\mathcal{N}_-.\end{aligned} \tag{8}$$

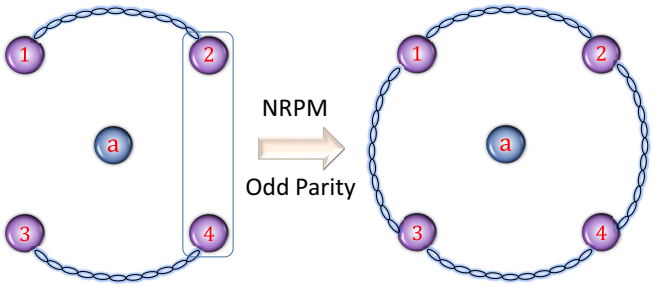

FIG. 3. Schematic of the entangled state fusion via the proposed NRPM. The connected chain denotes entanglement. Left panel: Atoms 1 and 2, 3 and 4 are initially in the nonmaximal entangled state with the same form $\alpha|00\rangle + \beta|11\rangle$. Auxiliary atom a is initially in state $|+\rangle$. Right panel: Four-body maximal entangled state induced by the NRPM due to the odd-parity measurement result.

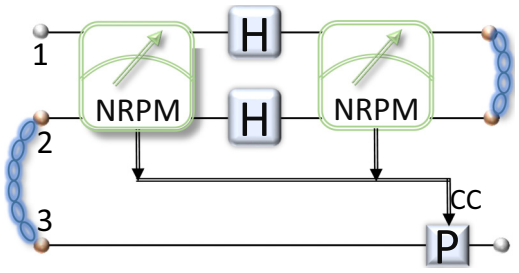

FIG. 4. Diagram of quantum teleportation based on the proposed NRPM, where Alice owns Rydberg atoms 1 and 2, and Bob owns Rydberg atom 3. The state to be teleported is prepared in atom 1. Atoms 2 and 3 are initially entangled with each other. H and CC indicate a single-qubit Hadamard gate and classical communication, respectively. P denotes the identity matrix or one of the Pauli matrices based on the results of NRPMs.

Therefore, after the above three steps, the parity information of the qubit atoms is acquired in a nondestructive manner from the measurement result of the atom a. In what follows, we focus on discussing the potential applications of this NRPM proposal.

III. APPLICATIONS OF THE NRPM

A. Fusion of entangled states

Motivated by a previous work [31], now we discuss how to fuse the two-body nonmaximally entangled states into a four-body maximally entangled state via the proposed NRPM. As presented in Fig. 3 with two groups of the Rydberg atoms 1, 2 and 3, 4 initially in the state

$$|\phi\rangle = (\alpha|00\rangle_{12} + \beta|11\rangle_{12}) \otimes (\alpha|00\rangle_{34} + \beta|11\rangle_{34}), \quad (9)$$

the parity meter applied on the atoms 2 and 4 yields the whole state to be collapsed to

$$|\phi\rangle = (|0011\rangle_{1234} + |1100\rangle_{1234})/\sqrt{2}, \quad (10)$$

for odd parity with the probability $2\alpha^2\beta^2$ and to

$$|\phi\rangle = (\alpha^2|0000\rangle_{1234} + \beta^2|1111\rangle_{1234})/\sqrt{\alpha^4 + \beta^4} \quad (11)$$

for even parity with the probability $\alpha^4 + \beta^4$. Equation (10) is for a four-qubit maximally entangled state. If we discard the nonmaximal entangled state in Eq. (11), the success probability of this scheme is simply $2(\alpha\beta)^2$.

B. Quantum teleportation in Rydberg atoms

We first show below how to achieve the Bell state analysis in Rydberg atom platform via the proposed NRPM based on the viewpoint of Ref. [32]. For four orthogonal Bell states

$$|\Psi^{\pm}\rangle = \frac{1}{\sqrt{2}}(|00\rangle \pm |11\rangle), |\Phi^{\pm}\rangle = \frac{1}{\sqrt{2}}(|01\rangle \pm |10\rangle), \quad (12)$$

the NRPM could distinguish $|\Psi^{\pm}\rangle$ from $|\Phi^{\pm}\rangle$ since the former are of even parity while the latter's parity is odd. Then we perform Hadamard gates on these two qubits, which makes the transitions

$$|\Psi^+\rangle \to |\Psi^+\rangle, \quad |\Psi^-\rangle \to |\Phi^+\rangle,$$
$$|\Phi^+\rangle \to |\Psi^+\rangle, \quad |\Phi^-\rangle \to |\Phi^-\rangle, \quad (13)$$

and then we perform the NRPM again. After other two Hadamard gates are performed, the state of the system is back to the initial state. Combining the results of these two parity meters, we acquire the information of the initial Bell states without destroying them.

We now apply the basic idea of complete-Bell-state-analysis-based quantum teleportation [33] to the Rydberg atom platform using the proposed NRPM. As shown in Fig. 4, the state to be teleported is initially prepared in atom 1 as $|\psi\rangle = \alpha|0\rangle_1 + \beta|1\rangle_1$. Our first step is to prepare an Einstein-Podolsky-Rosen (EPR) pair between two Rydberg atoms, which can be accomplished by photons as a quantum bus [34] or by quantum repeaters [35]. In this way, we have atoms 2 and 3 initially in $|\Psi^+\rangle = (|00\rangle_{23} + |11\rangle_{23})/\sqrt{2}$. Then we involve Alice and Bob, with the former sending her qubit information to the latter. As such, Alice performs the NRPM two times, with two single-qubit operations in between. Then Alice tells Bob the results of the two NRPMs through classical communication, based on which Bob performs single-qubit operations accordingly to reproduce the state $|\psi\rangle$. The one-to-one match between the results of the NRPMs and single-qubit operations is listed in Table. I.

C. Decoherence-free subspace quantum information processing

Single-logic-qubit operations. The dephasing error, which stems from the uncontrolled action of exterior fields and

TABLE I. One-to-one match between the results of the NRPMs and single-qubit operations.

First NRPM	Second NRPM	Single-qubit operation
Even	Even	$\hat{I}$
Even	Odd	σ_z
Odd	Even	σ_x
Odd	Odd	$\sigma_z\sigma_x$

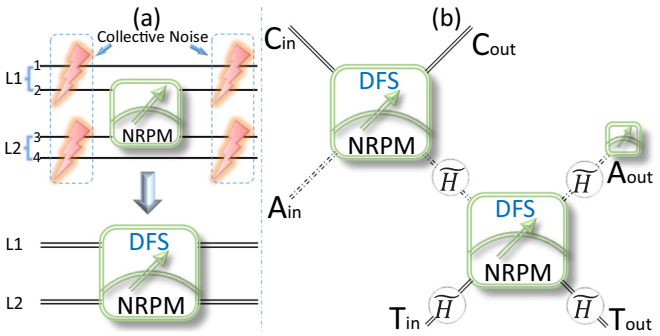

FIG. 5. (a) Diagram of NRPM in collective-dephasing DFS, where L1 and L2 denote the logical qubits. (b) Diagram of controlled-NOT in DFS, where $C_{\rm in}$ and $C_{\rm out}$, $A_{\rm in}$ and $A_{\rm out}$, and $T_{\rm in}$ and $T_{\rm out}$ represent the input and output states of the controlled, auxiliary, and target qubits, respectively. $\tilde{H}$ denotes the Hadamard gate operation in DFS.

mainly determines T_2, may have more influence on the fidelity of the Rydberg-atom-based schemes than other factors determining T_1. Here we suppose the Rydberg atoms subject to the collective dephasing error and consider the DFS by the encoding $|\tilde{0}\rangle = |01\rangle$ and $|\tilde{1}\rangle = |10\rangle$ [36]. The arbitrary z rotation $\tilde{U}_z$ on a single-logic-qubit, i.e., $\tilde{U}_z(\alpha)|\tilde{0}\rangle = e^{-i\alpha}|\tilde{0}\rangle$ and $\tilde{U}_z(\alpha)|\tilde{1}\rangle = e^{i\alpha}|\tilde{1}\rangle$, can be accomplished by rf pulses or Raman transition on the first physical qubit (i.e., the individual Rydberg atom) [37]. Another important single-logic-qubit operation is the Hadamard gate, which can be implemented as $\tilde{H} = C_{\rm NOT}^{\rm f,s} H_{\rm f} C_{\rm NOT}^{\rm f,s}$, where $C_{\rm NOT}^{\rm f,s}$ is the controlled-NOT gate with the first (second) atom being the control (target) qubit. $H_{\rm f}$ is the Hadamard gate on the first Rydberg atom.

Rydberg parity meter in DFS. To construct the controlled-NOT gate in DFS, we first construct a NRPM in this DFS, as shown in Fig. 5(a). Using the NRPM proposed in Sec. II, we suppose that the state in DFS is initially prepared as $|\psi\rangle_{L1} = p|\tilde{0}\rangle + q|\tilde{1}\rangle \equiv p|01\rangle_{12} + q|10\rangle_{12}$ and $|\psi\rangle_{L2} = m|\tilde{0}\rangle + n|\tilde{1}\rangle \equiv m|01\rangle_{34} + n|10\rangle_{34}$. Thus the system is in the state of $|\psi\rangle_L = pm|0101\rangle + pn|0110\rangle + qm|1001\rangle + qn|1010\rangle$. After applying the parity meter on the physical qubits (i.e., the Rydberg atoms) 2 and 3, we have the odd parity of the atoms 2 and 3, i.e., $pm|0101\rangle + qn|1010\rangle$, corresponding to the even-parity state in DFS and *vice versa*.

*Controlled-*NOT *gate in DFS.* Following the spirit of Refs. [19,20], we show how to use the NRPM to construct the controlled-NOT gate in DFS. We suppose that the input state of the control qubit in DFS is prepared in $a|\tilde{0}\rangle_C + b|\tilde{1}\rangle_C$, $A_{\rm in}$ is prepared in the state $(|\tilde{0}\rangle_A + |\tilde{1}\rangle_A)/\sqrt{2}$, and $T_{\rm in}$ is prepared in the state $c|\tilde{0}\rangle_T + d|\tilde{1}\rangle_T$. The whole state of the system is

$$|\tilde{\psi}\rangle = \frac{1}{\sqrt{2}}(a|\tilde{0}\rangle_C + b|\tilde{1}\rangle_C) \otimes (|\tilde{0}\rangle_A + |\tilde{1}\rangle_A) \otimes (c|\tilde{0}\rangle_T + d|\tilde{1}\rangle_T). \quad (14)$$

Following the process in Fig. 5(b), if the first NRPM in DFS is of even parity, the whole state would collapse to

$$|\tilde{\psi}\rangle = (a|\tilde{0}\tilde{0}\rangle_{CA} + b|\tilde{1}\tilde{1}\rangle_{CA}) \otimes (c|\tilde{0}\rangle_T + d|\tilde{1}\rangle_T). \quad (15)$$

TABLE II. Measurement results of NRPMs and $A_{\rm out}$ in DFS, and the corresponding single-logical qubit operations on $T_{\rm out}$ and $C_{\rm out}$ to achieve the controlled-NOT gate in DFS. $\hat{\sigma}_j^C$ and $\hat{\sigma}_j^T$ denote $\hat{\sigma}_j$ operation on the control and target logical qubits, respectively.

First NRPM	Second NRPM	$A_{\rm out}$	Single-qubit operation
Even	Even	$\|\tilde{0}\rangle$	$\hat{I}$
Even	Even	$\|\tilde{1}\rangle$	$\hat{\sigma}_x^T$
Even	Odd	$\|\tilde{0}\rangle$	$\hat{\sigma}_z^C$
Even	Odd	$\|\tilde{1}\rangle$	$\hat{\sigma}_z^C\hat{\sigma}_x^T$
Odd	Even	$\|\tilde{0}\rangle$	$\hat{\sigma}_x^T$
Odd	Even	$\|\tilde{1}\rangle$	$\hat{I}$
Odd	Odd	$\|\tilde{0}\rangle$	$\hat{\sigma}_z^C\hat{\sigma}_x^T$
Odd	Odd	$\|\tilde{1}\rangle$	$\hat{\sigma}_z^C$

After $\tilde{H}$ operations are carried out on the auxiliary and target logical qubits, respectively, the system qubit would be

$$|\tilde{\psi}\rangle = \tfrac{1}{2}[a|\tilde{0}\rangle_C(|\tilde{0}\rangle + |\tilde{1}\rangle)_A + b|\tilde{1}\rangle_C(|\tilde{0}\rangle - |\tilde{1}\rangle_A)] \otimes [c(|\tilde{0}\rangle + |\tilde{1}\rangle)_T + d(|\tilde{0}\rangle - |\tilde{1}\rangle_T)]. \quad (16)$$

If the result of the second NRPM in DFS is of even parity, the state would collapse to

$$|\tilde{\psi}\rangle = (ac + ad)|\tilde{0}\tilde{0}\tilde{0}\rangle_{\rm CAT} + (ac - ad)|\tilde{0}\tilde{1}\tilde{1}\rangle_{\rm CAT} + (bc + bd)|\tilde{1}\tilde{0}\tilde{0}\rangle_{\rm CAT} - (bc - bd)|\tilde{1}\tilde{1}\tilde{1}\rangle_{\rm CAT}. \quad (17)$$

We perform the Hadamard gates on the auxiliary and target qubits and then measure the output state of the auxiliary logical qubit. For the result of $A_{\rm out}$ to be $|\tilde{0}\rangle$, the final output state of the control and target logical qubits would be

$$|\tilde{\psi}\rangle = ac|\tilde{0}\tilde{0}\rangle_{CT} + ad|\tilde{0}\tilde{1}\rangle_{CT} + bc|\tilde{1}\tilde{1}\rangle_{CT} + bd|\tilde{1}\tilde{0}\rangle_{CT}, \quad (18)$$

indicating the success of the controlled-NOT operation.

In above paragraph, we consider only one case for the results of NRPM in DFS and $A_{\rm out}$. For the other measurement results, the controlled-NOT gate would also be successful when the appropriate single-logical qubit operation is performed on the state of $T_{\rm out}$, as shown in Table II.

Reference [38] proposed a scheme to realize universal quantum computation in collective-dephasing DFS of the Rydberg atoms. In contrast to the seminal one-step scheme in Ref. [38], the present multiple-step scheme, as one of the applications of the proposed NRPM, is based on the second-order perturbation dynamics rather than the fourth-order perturbation dynamics, which may relax restrictions for some parameters and reduce the evolution time.

Other potential applications in DFS. As discussed in Secs. III A and III B, the parity meter can also be used to fuse the entangled state [31], realize Bell-state analysis [32], and perform quantum teleportation [33]. With the similar process, the parity-meter constructed in DFS can be used to accomplish the same quantum information tasks in DFS. In addition, as a basic building block in quantum information [31], the parity

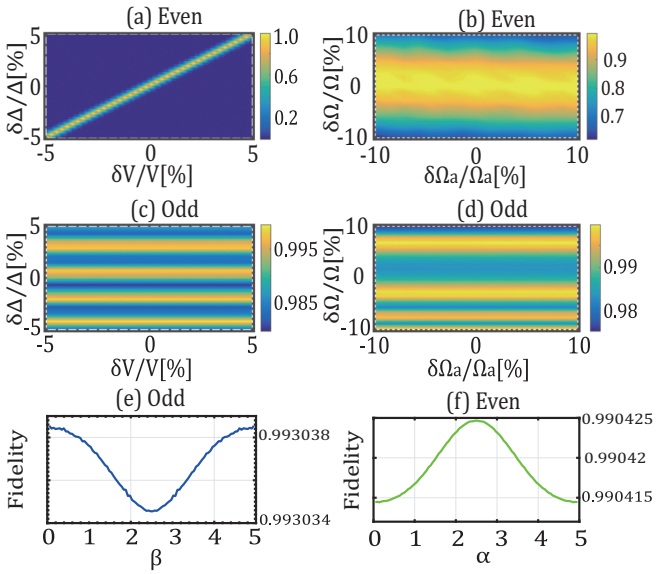

FIG. 6. (a)–(d): Fidelities of even- and odd-parity cases versus the fluctuations of characteristic parameters, in which we set $\alpha = \beta = \gamma = \delta = 0.5$. (e) Fidelity of odd-parity case versus β, where we set $\gamma = 5 - \beta$, $\alpha = \delta = 0.5$. (f) Fidelity of even-parity case versus α, where we set $\delta = 5 - \alpha$, $\beta = \gamma = 0.5$. The rest parameters are chosen as $\Omega/2\pi = 10$ MHz, $\Omega_a = \Omega$, $\Delta = 10\Omega$, $V = 2\Delta$, $V' = 0$, $\gamma_R = \gamma_r = 2$ kHz.

meter designed here can also be considered to construct a quantum network in DFS.

IV. DISCUSSION

Performance of the NRPM. To evaluate the fidelity and probability of the presented NRPM, we set the initial state as $|\psi\rangle = (\alpha|00\rangle + \beta|01\rangle + \gamma|10\rangle + \delta|11\rangle)/\mathcal{N}$ with $\mathcal{N}$ being the normalized parameter. The ideal even- and odd-parity states after the NRPM are, respectively, $|\psi\rangle_{\text{even}} = (\alpha|00\rangle + \delta|11\rangle)/\sqrt{\alpha^2 + \delta^2}$ and $|\psi\rangle_{\text{odd}} = (\beta|01\rangle + \gamma|10\rangle)/\sqrt{\beta^2 + \gamma^2}$. The system evolves under the government of the Lindblad master equation,

$$\dot{\hat{\rho}}(t) = -i[\hat{H},\ \hat{\rho}] + \sum_{\epsilon=0,1}\sum_{\zeta=1,2,a}\sum_{\eta=R,r}\hat{\mathcal{L}}[\hat{\sigma}_{\epsilon,\zeta,\eta}], \tag{19}$$

where

$$\hat{\mathcal{L}}[\hat{\sigma}_{\epsilon,\zeta,\eta}] = \tfrac{1}{2}(2\hat{\sigma}_{\epsilon,\zeta,\eta}\hat{\rho}\hat{\sigma}^{\dagger}_{\epsilon,\zeta,\eta} - \hat{\sigma}^{\dagger}_{\epsilon,\zeta}\hat{\sigma}_{\epsilon,\zeta,\eta}\hat{\rho} - \hat{\rho}\hat{\sigma}^{\dagger}_{\epsilon,\zeta,\eta}\hat{\sigma}_{\epsilon,\zeta,\eta}) \tag{20}$$

denotes the Lindblad operators and $\hat{\sigma}_{\epsilon,\zeta,\eta} = \sqrt{\gamma_\eta/2}|\epsilon\rangle_\zeta\langle\eta|$ denotes the spontaneous emission process from $|\eta\rangle$ to $|\epsilon\rangle$ of atom ζ with the rate $\gamma_\eta/2$. In Figs. 6(a) and 6(b) we plot the fidelities of the parity meter (even-parity result) versus parameter fluctuations with the definition of $F = \text{Tr}[\hat{\rho}(t)|\psi\rangle_{\text{even}}\langle\psi|]/[(\alpha^2 + \delta^2)/(\alpha^2 + \beta^2 + \gamma^2 + \delta^2)]$. The odd-parity cases with the definition of $F = \text{Tr}[\hat{\rho}(t)|\psi\rangle_{\text{odd}}\langle\psi|]/[(\beta^2 + \gamma^2)/(\alpha^2 + \beta^2 + \gamma^2 + \delta^2)]$ are shown in Figs. 6(c) and 6(d). Since the antiblockade condition should be well satisfied for the even parity, the fidelity in Fig. 6(a) is more sensitive to the parameter (Δ and V) fluctuation than that in Fig. 6(c). Even so, the fidelity may still be larger than 0.97 when both of the fluctuations are about 5%. In Figs. 6(b) and 6(d) one can see that the influence of Ω fluctuation is greater than that of Ω_a fluctuation. That is because the physical process relevant to Ω is the second-order dynamical process guided by the square of Ω and Δ, while the physical process relevant to Ω_a is the resonant coupling process. In Figs. 6(e) and 6(f), we plot the fidelities of the NRPM in a wide range of coefficients, which show the stability of fidelity. In Fig. 6 the errors and the infidelity are mainly caused by the antiblockade error ($|01\rangle$ and $|10\rangle$ state would also be excited even under the large detuning situation) in steps (i) and (iii), blockade error in step (ii), and atomic spontaneous emission. To suppress the antiblockade error, one can select Rydberg states with slightly stronger Rydberg interactions and/or larger detunings Δ_R and Δ_r. To reduce the blockade error, one may consider the methods employed in Refs. [39]. For the error induced by atomic spontaneous emission, one may employ higher-lying Rydberg states in lower temperature, which could enlarge the lifetime.

Experimental considerations. We now summarize the requirements for the Rydberg states in experiments. First, the dipole-dipole interaction should be minimized to be weak enough and the vdW interaction should play the main role. In order to make V_{dd} in Eq. (4) negligible, one can choose both of the Rydberg states $|R\rangle$ and $|r\rangle$ in the s orbital due to the selection rules. Also, to suppress the dipole-dipole interaction between any of these two Rydberg states ($|R\rangle$ and $|r\rangle$) and any other Rydberg states, one should set the interatomic distance larger than the characteristic distance R_c [2]. Second, in steps (i) and (iii), the diagonal vdW interaction strength V should be bigger than off-diagonal vdW interaction strength V' to make the condition $V - V' \gg \Omega$ feasible ($V = 2\Delta$; for the dynamics please see Fig. 2). This requirement could be fulfilled by encoding $|R\rangle$ and $|r\rangle$ into different Zeeman sublevels [30]. As well, if the principal quantum numbers of $|R\rangle$ and $|r\rangle$ are very different from each other, the requirement $V_{RR}(V_{rr}) - V' \gg \Omega$ could also be fulfilled (we still suppose $V_{Rr} = V_{rR} = V'$ for simplicity) [40]. However, the condition $V_{RR} = V_{rr}$ may not be satisfied in this case because the vdW interaction typically scales as n^{11} (n denotes the principal quantum number) [2], which invalidates Eq. (5). Moreover, in step (ii) the condition $V' \ll \Omega_a$ is also required.

Now we check some more complicated cases in actual implementation of our scheme. First, for $V_{RR} \neq V_{rr}$, we have to modify some relevant parameters. V_{RR} and V_{rr} could be known if the energy levels of $|R\rangle$ and $|r\rangle$, the quantization axis as well as the external fields, are determined. Suppose the condition $\{V_{RR},\ V_{rr}\} \gg \{\Omega_r,\ \Omega_R\}$ is still satisfied when $V_{RR} \neq V_{rr}$. With the conditions $\Delta_R = V_{RR}/2$, $\Delta_r = V_{rr}/2$ and $V_{RR}\,(V_{rr}) - V' \gg \Omega$, the effective Hamiltonian in Eq. (4) would be modified to

$$\begin{aligned}\hat{H}_{\text{eff}} = {} & \frac{\Omega_R^2}{2\Delta_R}|00\rangle\langle RR| + \frac{\Omega_r^2}{2\Delta_r}|11\rangle\langle rr| + \text{H.c.} \\ & + \frac{\Omega_R^2}{4\Delta_R}[2|00\rangle\langle 00| + |01\rangle\langle 01| + |10\rangle\langle 10|] \\ & + \frac{\Omega_r^2}{4\Delta_r}[2|11\rangle\langle 11| + |01\rangle\langle 01| + |10\rangle\langle 10|].\end{aligned} \tag{21}$$

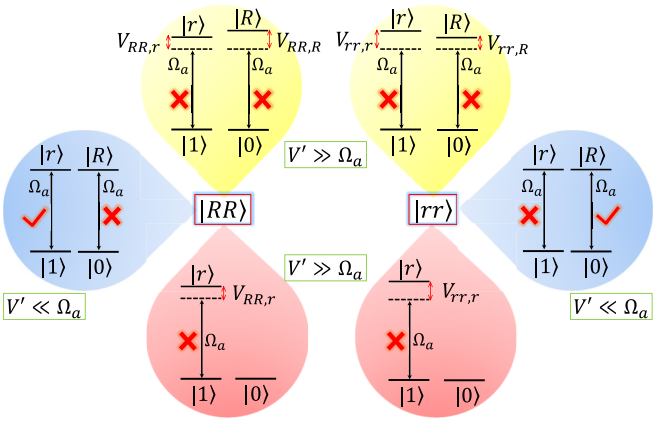

FIG. 7. Schematic of the auxiliary atom's excitation in step (ii) conditional on the qubit atoms in $|RR\rangle$ or $|rr\rangle$. $V_{jj,k}$ ($\{j,\ k\} \in \{r,\ R\}$) denotes the RRI strength between the qubit atoms' states $|jj\rangle$ and the auxiliary atom's state $|k\rangle$. Two horizontal circles denote the case $V' \ll \Omega_a$ in Sec. II. The upper two circles indicate the failure of the scheme due to the unwanted blockade induced by $V' \gg \Omega_a$, which yields the output state of the auxiliary atom as $|+\rangle_a$. However, as we have shown in step (ii) of Sec. II, the output state of auxiliary atom should be $|-\rangle_a$ conditional on the systematic qubit in $|RR\rangle$ or $|rr\rangle$, and thus the scheme would not work. The bottom two circles show how to address the issue for the case $V' \gg \Omega_a$ via turning off the driving lasers acting on $|0\rangle \to |R\rangle$ of the auxiliary atom. For the former case in the horizontal circles, the measurement result $|+\rangle_a$ ($|-\rangle_a$) corresponds to the odd (even) parity. But for the cases in bottom circles, the measurement result $|+\rangle_a$ ($|-\rangle_a$) corresponds to the even (odd) parity.

If we set $\Omega_R^2/\Delta_R = \Omega_r^2/\Delta_r = \Omega_{\rm eff}$ and ignore the global phase, Eq. (21) is reduced to

$$\hat{H}_{\rm eff} = \Omega_{\rm eff}(|00\rangle\langle RR| + |11\rangle\langle rr| + \text{H.c.}), \tag{22}$$

which is of the same form as Eq. (5). However, the state $|RR\rangle$ ($|rr\rangle$) would acquire a phase $V_{RR}t_a$ ($V_{rr}t_a$) in step (ii), which would move to the state of $|00\rangle$ ($|11\rangle$) after step (iii). Then, if the measurement result is of even parity, the system state would collapse to $[e^{-i(V_{RR}-V_{rr})t_a}a|00\rangle + d|11\rangle]/\sqrt{2}$. One can perform single-qubit operations $|0\rangle \to e^{-i(V_{RR}-V_{rr})t_a/2}|0\rangle$ [or $|1\rangle \to e^{-i(V_{RR}-V_{rr})t_a/2}|1\rangle$] on both atoms to cancel the phase. Moreover, the mechanical effect would be induced when two qubit atoms are both in Rydberg states in step (ii). The way to minimize this effect is to enhance the strength of Ω_a properly, which would shorten the time of step (ii).

The previously assumed condition $V' \ll \Omega_a$ is not always satisfied experimentally. As long as $\Delta_R + \Delta_r - V' \gg \Omega$ is satisfied, however, the effective Hamiltonian in Eq. (22) for steps (i) and (iii) is invariant. Nevertheless, the dynamical process in step (ii) would be affected greatly because when $V' \ll \Omega_a$ is not satisfied, the qubit state $|RR\rangle$ ($|rr\rangle$) would also block the excitation process $|1\rangle \to |r\rangle$ ($|0\rangle \to |R\rangle$) of the auxiliary atom. To address this issue, one can modulate the couplings of the auxiliary atom, as shown in the two bottom circles of Fig. 7.

The main differences and connections of the parity meters between ours and in Refs. [27,28] can be summarized as follows. (i) The parity meter used in Ref. [27] is to measure the many-body parity between the ground state and the Rydberg state, while our proposed parity meter is constructed to measure the two-body parity in ground-state subspace in a nondestructive manner. (ii) The scheme in Ref. [28] employs the four-body parity constraints (odd-parity states as the ground state of the specified Hamiltonian) to realize the coherent quantum annealer, in which the auxiliary atom is used to compensate two associated energies, make odd-parity states degenerate, and further implement the four-body constraints. Whereas in our scheme, the auxiliary atom is used to measure the parity information of the two qubit atoms, which is the reason that our scheme is nondestructive. (iii) In our scheme, the two-body parity is exactly the two-body case of the many-body parity with operator $\mathcal{P} = \prod_i \sigma_z^i$ [27].

For a concrete experimental process, we may consider the excitation from the ground state to the Rydberg state achieved by a two-photon process [10–18] or single-photon process [41] in Rb and Cs atom platforms, respectively, with the corresponding ground state encoding $\{|0\rangle = |5S_{1/2},\ F = 2,\ m_F = 0\rangle,\ |1\rangle = |5S_{1/2},\ F = 1,\ m_F = 0\rangle\}$ for the Rb atom and $\{|0\rangle = |6S_{1/2},\ F = 3,\ m_F = 0\rangle,\ |1\rangle = |6S_{1/2},\ F = 4,\ m_F = 0\rangle\}$ for the Cs atom. For a two-photon process in a Rb atom platform, the intermediate state $|p\rangle = |5P_{3/2}\rangle$ is employed to complete the excitation process. The Rydberg state could be chosen as $|R\rangle \equiv |60S_{1/2}, m_j = 1/2\rangle$ and $|r\rangle \equiv |57S_{1/2}, m_j = 1/2\rangle$. The C_6 parameters [40,42] for V_{RR}, V_{rr}, and V_{Rr} (V_{rR}) are assumed to be about 135 GHz μm^6, 74 GHz μm^6, and -44 GHz μm^6, respectively. If the Rydberg atoms are located by a center-to-center distance of 3 μm away, the vdW interaction may play a main role and the RRI strengths V_{RR}, V_{rr}, and $V_{Rr}(V_{rR})$ would be $2\pi \times 29.488$ MHz, $2\pi \times 16.164$ MHz, and $2\pi \times (-9.611)$ MHz, respectively. In addition, we may assume $\Delta_R = V_{RR}/2$, $\Delta_r = V_{rr}/2$, $\Delta_R = 10\Omega_R$, $\Omega_R^2/\Delta_R = \Omega_r^2/\Delta_r$, and $\Omega_a = \Omega_R$, which indicates $\Omega_R \approx 2\pi \times 1.4737$ MHz, $\Omega_r \approx 2\pi \times 1.0911$ MHz, $\Delta_R \approx 2\pi \times 14.737$ MHz, and $\Delta_r \approx 2\pi \times 8.078$ MHz.

We plot the two-photon process in Fig. 8(a), in which the parameters have the following relations with the qubit atom in Fig. 1: $\Omega_R = \Omega_{0p}\Omega_{pR}[1/(2\Delta_{p0}) + 1/(2\Delta_{p0} - 2\Delta_{R0})]$, $\Omega_r = \Omega_{1p}\Omega_{pr}[1/(2\Delta_{p1}) + 1/(2\Delta_{p1} - 2\Delta_{r1})]$, and $\Delta_R = \Delta_{R0}$, $\Delta_r = \Delta_{r1}$. Without loss of generality, one can set $\Delta_{p0} = 4$ GHz, $\Delta_{R0} = 2\pi \times 14.737$ MHz, $\Omega_{0p} = 2\pi \times 60$ MHz, $\Omega_{pR} = 2\pi \times 15.5454$ MHz, $\Delta_{p1} = 5$ GHz, $\Delta_{r1} = 2\pi \times 8.078$ MHz, $\Omega_{1p} = 2\pi \times 80$ MHz, and $\Omega_{pr} = 2\pi \times 10.798$ MHz. If we suppose the laser waist to be 2.5 μm, then the laser power for Ω_{0p}, Ω_{pR}, Ω_{1p}, and Ω_{pr} could be about 0.04 μW, 527 μW, 0.06 μW, and 254 μW, respectively.

Also, the lifetimes for $|R\rangle$ and $|r\rangle$ are about [43] $\tau_R \approx 263$ μs and $\tau_r \approx 226$ μs, respectively, with the available temperature at the order of μK magnitude [3]. Using these parameters, we find the optimal fidelity of the odd- and even-parity cases to be 0.981 and 0.956, respectively, with the total time 7.84 μs. For the single-photon excitation process as scheduled in Fig. 8(b), the Rydberg states should be chosen in p orbit due to the selection rule, and we will not discuss it in detail here.

Improvement of the NRPM. The operation steps may be reduced provided that we can construct the three-qubit quantum gate

$$\hat{U}_3 = \text{diag}[-1, 1, 1, 1, 1, 1, 1, -1] \tag{23}$$

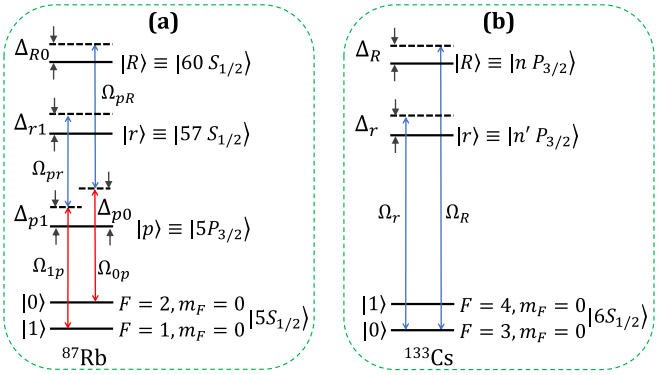

FIG. 8. Energy level scheme and laser driving process of a single qubit atom. (a) Two-photon process exemplified by ^{87}Rb. Ω_{0p} and Ω_{pR} denote the coupling strengths of $|0\rangle \to |p\rangle$ and $|p\rangle \to |R\rangle$, respectively. Δ_{R0} is the effective detuning for the two-photon process $|0\rangle \to |p\rangle \to |R\rangle$, during which the detuning Δ_{p0} is applied to the intermediate state $|p\rangle$. Ω_{1p} and Ω_{pr} denote the coupling strengths of $|1\rangle \to |p\rangle$ and $|p\rangle \to |r\rangle$, respectively. Δ_{r1} is the effective detuning for the two-photon process $|1\rangle \to |p\rangle \to |r\rangle$, during which the detuning Δ_{p1} is applied to $|p\rangle$. (b) Single-photon process to implement the scheme, exemplified by ^{133}Cs.

with the basis $\{|000\rangle, |001\rangle, |010\rangle, |011\rangle, |100\rangle, |101\rangle, |110\rangle, |111\rangle\}$ in a single step. In the following, we first show how to use $\hat{U}_3$ to achieve the NRPM and then show how to construct $\hat{U}_3$ in a single step. After performing $\hat{U}_3$, the initial state in Eq. (6) would evolve as

$$\begin{aligned}&(\alpha|00\rangle + \beta|01\rangle + \gamma|10\rangle + \delta|11\rangle)_{12} \otimes (|0\rangle + |1\rangle)_a \\ &\xrightarrow{\hat{U}_3} (-\alpha|00\rangle + \delta|11\rangle)_{12} \otimes (|0\rangle - |1\rangle)_a \\ &\quad + (\beta|01\rangle + \gamma|10\rangle)_{12} \otimes (|0\rangle + |1\rangle)_a. \end{aligned} \tag{24}$$

Then the parity information of the qubit atom is achieved after measuring the auxiliary atom with the basis $\{|+\rangle_a, |-\rangle_a\}$ and performing a single-qubit operation on one of the qubit atoms if the auxiliary atom is measured in $|-\rangle_a$ state. We now show how to construct $\hat{U}_3$ in a single step without requiring atomic individual addressing. As shown in Fig. 9(a), we consider three identical atoms. Each of the atoms is identical to the qubit atom in Fig. 1. The Hamiltonian of the whole system is given by

$$\begin{aligned}\hat{H} = &\sum_{j=1,2,a} \left(\frac{\Omega_R}{2} |0\rangle_j\langle R| e^{i\Delta_R t} + \frac{\Omega_r}{2} |1\rangle_j\langle r| e^{i\Delta_r t} + \text{H.c.} \right) \\ &+ V_{RR}(|RR\rangle_{12}\langle RR| + |RR\rangle_{1a}\langle RR| + |RR\rangle_{2a}\langle RR|) \\ &+ V_{rr}(|rr\rangle_{12}\langle rr| + |rr\rangle_{1a}\langle rr| + |rr\rangle_{2a}\langle rr|) \\ &+ V_{Rr}(|Rr\rangle_{12}\langle Rr| + |Rr\rangle_{1a}\langle Rr| + |Rr\rangle_{2a}\langle Rr|) \\ &+ V_{rR}(|rR\rangle_{12}\langle rR| + |rR\rangle_{1a}\langle rR| + |rR\rangle_{2a}\langle rR|). \end{aligned} \tag{25}$$

If the conditions $\Delta_R = V_{RR} + \Omega_R^2/(4\Delta_R)$, $\Delta_r = V_{rr} + \Omega_r^2/(4\Delta_r)$, $\{\Delta_R, \Delta_r\} \gg \{\Omega_R, \Omega_r\}$, and $\Delta_R + \Delta_r \gg 2V_{Rr}$ are fulfilled [44], the effective form of Eq. (25) would be

$$\hat{H}_{\text{eff3}} = \frac{3\Omega_R^3}{4\Delta_R^2}|000\rangle\langle RRR| + \frac{3\Omega_r^3}{4\Delta_r^2}|111\rangle\langle rrr| + \text{H.c.} \tag{26}$$

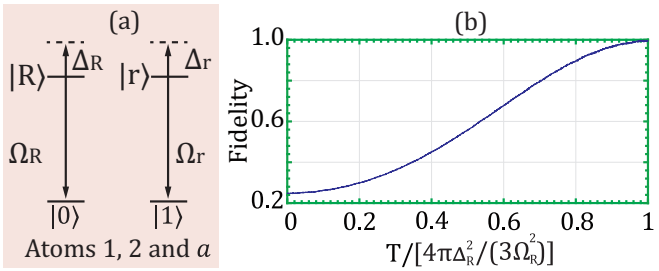

FIG. 9. (a) Energy-level scheme and laser driving process for atoms 1, 2 and a to construct $\hat{U}_3$ in a single step without atomic individual addressing. (b) Fidelity of $\hat{U}_3$ with respect to the evolution time. The system is initially in the state $|\psi\rangle = (|000\rangle + |001\rangle + |010\rangle + |011\rangle + |100\rangle + |101\rangle + |110\rangle + |111\rangle)/2\sqrt{2}$ and would evolve finally to $\hat{U}_3|\psi\rangle$ in an ideal case. The parameters are set as $\Omega_R = 1.5\Omega_r$, $\gamma_R = \gamma_r = 0.25 \times 10^{-4}\Omega_r$, $\Delta_r = 12\Omega_r$, $\Delta_R = \sqrt{\Omega_R^3/\Omega_r^3}\Delta_r$, $V_{RR} = \Delta_R - \Omega_R^2/(4\Delta_R)$, $V_{rr} = \Delta_r - \Omega_r^2/(4\Delta_r)$, and $V_{Rr} = V_{rR} = 0.5V_{rr}$.

after canceling the Stark shifts with the methods shown in Ref. [44]. Then, if the condition $\Omega_R^3/\Delta_R^2 = \Omega_r^3/\Delta_r^2$ is satisfied, $\hat{U}_3$ would be achieved after a 2π pulse. In Fig. 9(b) we plot the fidelity of $\hat{U}_3$ through numerically solving the master equation based on the full Hamiltonian in Eq. (25) with a group of specific initial states.

The main feature of the scheme to construct $\hat{U}_3$ is that the scheme can be implemented in one step without the requirement of atomic individual addressability. Thus the operation steps of $\hat{U}_3$-based NRPM may be largely simplified.

V. CONCLUSION

In summary, we have proposed a scheme to construct the NRPM and explored the possible applications. The main feature is that the parity meter constructed in ground-state subspace is nondestructive and can be used as a basic building block in Rydberg-atom-based quantum information science. The actual operations of the NRPM may suffer from imperfections due to parameter fluctuation and technical limitations, which were not fully considered in our treatment. Nevertheless, we believe that the present scheme for the nondestructive parity meter using Rydberg atoms may open a new path towards Rydberg-atom based quantum information processing.

ACKNOWLEDGMENTS

S.L.S. would like to thank Prof. Klaus Mølmer for valuable discussions of the initial idea during his visit to Aarhus University. The authors would like to thank Xiao-Feng Shi for useful comments and suggestions. This work was supported by the National Natural Science Foundation of China (NSFC) under Grants No. 11804308, 11835011, 11804375, 11734018, and 11674360.

[1] T. F. Gallagher, *Rydberg Atoms*, Vol. 3 (Cambridge University Press, Cambridge, 2005).

[2] M. Saffman, T. G. Walker, and K. Mølmer, Rev. Mod. Phys. **82**, 2313 (2010).

[3] M. Saffman, J. Phys. B: Atom. Mol. Opt. Phys. **49**, 202001 (2016).

[4] D. Comparat and P. Pillet, J. Opt. Soc. Am. B **27**, A208 (2010).

[5] L. Béguin, A. Vernier, R. Chicireanu, T. Lahaye, and A. Browaeys, Phys. Rev. Lett. **110**, 263201 (2013).

[6] D. Jaksch, J. I. Cirac, P. Zoller, S. L. Rolston, R. Côté, and M. D. Lukin, Phys. Rev. Lett. **85**, 2208 (2000).

[7] M. D. Lukin, M. Fleischhauer, R. Cote, L. M. Duan, D. Jaksch, J. I. Cirac, and P. Zoller, Phys. Rev. Lett. **87**, 037901 (2001).

[8] E. Urban, T. A. Johnson, T. Henage, L. Isenhower, D. Yavuz, T. Walker, and M. Saffman, Nat. Phys. **5**, 110 (2009).

[9] A. Gaëtan, Y. Miroshnychenko, T. Wilk, A. Chotia, M. Viteau, D. Comparat, P. Pillet, A. Browaeys, and P. Grangier, Nat. Phys. **5**, 115 (2009).

[10] L. Isenhower, E. Urban, X. L. Zhang, A. T. Gill, T. Henage, T. A. Johnson, T. G. Walker, and M. Saffman, Phys. Rev. Lett. **104**, 010503 (2010).

[11] X. L. Zhang, L. Isenhower, A. T. Gill, T. G. Walker, and M. Saffman, Phys. Rev. A **82**, 030306(R) (2010).

[12] T. Wilk, A. Gaëtan, C. Evellin, J. Wolters, Y. Miroshnychenko, P. Grangier, and A. Browaeys, Phys. Rev. Lett. **104**, 010502 (2010).

[13] K. M. Maller, M. T. Lichtman, T. Xia, Y. Sun, M. J. Piotrowicz, A. W. Carr, L. Isenhower, and M. Saffman, Phys. Rev. A **92**, 022336 (2015).

[14] Y. Zeng, P. Xu, X. He, Y. Liu, M. Liu, J. Wang, D. J. Papoular, G. V. Shlyapnikov, and M. Zhan, Phys. Rev. Lett. **119**, 160502 (2017).

[15] C. J. Picken, R. Legaie, K. McDonnell, and J. D. Pritchard, Quantum Sci. Technol. **4**, 015011 (2018).

[16] H. Levine, A. Keesling, A. Omran, H. Bernien, S. Schwartz, A. S. Zibrov, M. Endres, M. Greiner, V. Vuletić, and M. D. Lukin, Phys. Rev. Lett. **121**, 123603 (2018).

[17] H. Levine, A. Keesling, G. Semeghini, A. Omran, T. T. Wang, S. Ebadi, H. Bernien, M. Greiner, V. Vuletić, H. Pichler, and M. D. Lukin, Phys. Rev. Lett. **123**, 170503 (2019).

[18] T. M. Graham, M. Kwon, B. Grinkemeyer, Z. Marra, X. Jiang, M. T. Lichtman, Y. Sun, M. Ebert, and M. Saffman, Phys. Rev. Lett. **123**, 230501 (2019).

[19] C. W. J. Beenakker, D. P. DiVincenzo, C. Emary, and M. Kindermann, Phys. Rev. Lett. **93**, 020501 (2004).

[20] K. Nemoto and W. J. Munro, Phys. Rev. Lett. **93**, 250502 (2004).

[21] H.-A. Engel and D. Loss, Science **309**, 586 (2005).

[22] J.-W. Pan, C. Simon, Č. Brukner, and A. Zeilinger, Nature (London) **410**, 1067 (2001).

[23] B. Trauzettel, A. N. Jordan, C. W. J. Beenakker, and M. Büttiker, Phys. Rev. B **73**, 235331 (2006).

[24] D. Riste, M. Dukalski, C. Watson, G. De Lange, M. Tiggelman, Y. M. Blanter, K. W. Lehnert, R. Schouten, and L. DiCarlo, Nature (London) **502**, 350 (2013).

[25] L. Sun, A. Petrenko, Z. Leghtas, B. Vlastakis, G. Kirchmair, K. Sliwa, A. Narla, M. Hatridge, S. Shankar, J. Blumoff *et al.*, Nature (London) **511**, 444 (2014).

[26] J. Roffe, D. Headley, N. Chancellor, D. Horsman, and V. Kendon, Quant. Sci. Tech. **3**, 035010 (2018).

[27] A. Omran, H. Levine, A. Keesling, G. Semeghini, T. T. Wang, S. Ebadi, H. Bernien, A. S. Zibrov, H. Pichler, S. Choi *et al.*, Science **365**, 570 (2019).

[28] A. W. Glaetzle, R. M. van Bijnen, P. Zoller, and W. Lechner, Nat. Commun. **8**, 15813 (2017).

[29] Z. Zuo and K. Nakagawa, Phys. Rev. A **82**, 062328 (2010); T. E. Lee, H. Häffner, and M. C. Cross, Phys. Rev. Lett. **108**, 023602 (2012); W. Li, C. Ates, and I. Lesanovsky, *ibid.* **110**, 213005 (2013).

[30] A. W. Carr and M. Saffman, Phys. Rev. Lett. **111**, 033607 (2013); S.-L. Su, E. Liang, S. Zhang, J.-J. Wen, L.-L. Sun, Z. Jin, and A.-D. Zhu, Phys. Rev. A **93**, 012306 (2016); S.-L. Su, Y. Tian, H. Z. Shen, H. Zang, E. Liang, and S. Zhang, *ibid.* **96**, 042335 (2017); X. Q. Shao, J. H. Wu, and X. X. Yi, *ibid.* **95**, 062339 (2017); D. X. Li and X. Q. Shao, *ibid.* **99**, 032348 (2019).

[31] R. Ionicioiu, Phys. Rev. A **75**, 032339 (2007).

[32] J. Li, B.-S. Shi, Y.-K. Jiang, X.-F. Fan, and G.-C. Guo, J. Phys. B: Atom., Mol. Opt. Phys. **33**, 3215 (2000).

[33] Y.-H. Kim, S. P. Kulik, and Y. Shih, Phys. Rev. Lett. **86**, 1370 (2001).

[34] L. Sárkány, J. Fortágh, and D. Petrosyan, Phys. Rev. A **92**, 030303(R) (2015).

[35] B. Zhao, M. Müller, K. Hammerer, and P. Zoller, Phys. Rev. A **81**, 052329 (2010).

[36] M. Feng, Phys. Rev. A **63**, 052308 (2001); D. Kielpinski, C. Monroe, and D. J. Wineland, Nature (London) **417**, 709 (2002).

[37] P. Xue and Y.-F. Xiao, Phys. Rev. Lett. **97**, 140501 (2006).

[38] E. Brion, L. H. Pedersen, K. Mølmer, S. Chutia, and M. Saffman, Phys. Rev. A **75**, 032328 (2007).

[39] D. Petrosyan, F. Motzoi, M. Saffman, and K. Mølmer, Phys. Rev. A **96**, 042306 (2017); X.-F. Shi, Phys. Rev. Appl. **10**, 034006 (2018); **7**, 064017 (2017).

[40] R. M. W. van Bijnen, Quantum engineering with ultracold atoms, Ph.D. thesis, Eindhoven University of Technology, Eindhoven, 2013; D. Cano and J. Fortágh, Phys. Rev. A **89**, 043413 (2014); Y.-M. Liu, X.-D. Tian, D. Yan, Y. Zhang, C.-L. Cui, and J.-H. Wu, *ibid.* **91**, 043802 (2015).

[41] Y.-Y. Jau, A. Hankin, T. Keating, I. Deutsch, and G. Biedermann, Nat. Phys. **12**, 71 (2016).

[42] K. Singer, J. Stanojevic, M. Weidemüller, and R. Côté, J. Phys. B: Atom. Mol. Opt. Phys. **38**, S295 (2005).

[43] I. I. Beterov, I. I. Ryabtsev, D. B. Tretyakov, and V. M. Entin, Phys. Rev. A **79**, 052504 (2009).

[44] S. L. Su, H. Z. Shen, E. Liang, and S. Zhang, Phys. Rev. A **98**, 032306 (2018).